Segmentation and Anatomical Annotation of Cerebral Arteries in Non-Angiographic MRI

Bertram Sabrowsky-Hirsch [1,*], Philipp Moser [1], Stefan Thumfart [1], and Josef Scharinger [2]

[1] RISC Software GmbH, Hagenberg, Austria; Email: bertram.sabrowsky-hirsch@risc-software.at
[2] Johannes Kepler University, Linz, Austria; Email: josef.scharinger@jku.at
*Correspondence: bertram.sabrowsky-hirsch@risc-software.at

***Abstract*—The assessment of cerebrovascular disease benefits from the availability of different neuroimaging modalities, each providing different aspects to the vasculature and surrounding brain parenchyma. Segmented vasculature may improve cross-modal alignment but is difficult to annotate in sequences without vessel contrast. We propose a novel method to segment cerebral arteries in three non-angiographic sequences: T1w, T2w and PDw. Our method further predicts annotations for four anatomical regions, which can be used to mask specific parts of the vascular network or analyze the topology. For our experiments, we annotated arterial vessels and anatomical regions in 2,218 scans of the IXI dataset using a novel automatic method. We used the nnU-Net framework to train models in a 5-fold cross validation and to predict on a separate test-set. Our results suggest that vascular structures can be segmented and annotated in the examined MRI sequences with reasonable quality. The approach may potentially be used to study vascular diseases, when trained on pathological images. We share our ground-truth and models to encourage future experiments.**

***Keywords*—artificial intelligence, segmentation, magnetic resonance imaging, unet, cerebral arteries**

I. Introduction

Cerebrovascular disease comprises a group of disorders affecting the blood vessels supplying the brain, of which stroke is the second leading cause of death and a major cause of disability worldwide [17]. Neuroimaging has a critical role in stroke prevention [28], treatment [30] and recovery [22], all of which can benefit from vascular segmentations. Existing methods rely on angiographic imaging modalities developed to visualize vascular structures. However, in clinical practice, T1-, T2- and PD-weighted MRI are commonly available sequences included in the STRIVE acquisition standards [32].

A segmentation method for vascular structures in conventional non-angiographic MRI could be applied to a wide range of available medical image data and thus be used for retrospective studies and guidance in diagnosis. As an example, Dobrocky et al. [6] suggest the fusion of digital subtraction angiography (DSA) images and MRI to refine diagnoses and guide therapeutic decision-making. Aligning MRI with DSA images can be challenging due to low tissue contrast and different scan field sizes (DSA scans are typically smaller to reduce radiation exposure [7]).

Segmented vasculature in MRI could guide the manual alignment or serve as a registration target. We further suggest annotating the segmented vasculature, however, contrary to previous approaches which labeled individual segments of arterial vessels [29,10], we propose to annotate anatomical regions based on circulation instead.

Anterior and posterior circulation are differentiated for the clinical management of strokes [26]. Within the anterior circulation, we distinguish vasculature of the middle (MCA) and anterior (ACA) cerebral arteries. Thus, we define four anatomical regions: left and right comprise the respective ICA and MCA; posterior includes the basilar (BA) and posterior (PCA) arteries; anterior starts at the A1 segments and includes the ACA. We believe that the proposed regions better accommodate for the variable nature of the Circle-of-Willis (CoW), where individual segments may not be present or exist as duplicates. Furthermore, labeled circulatory regions are useful for aligning DSA images, where vasculature is only visible in the circulation of a primary artery injected with contrast agent.

In this paper we introduce a novel method to segment and annotate cerebral arteries in four different MRI sequences: TOF MRA, T1w, T2w and PDw. We first present a fully automatic method to generate ground-truth from TOF MRAs using atlas- and graph-based methods. The ground-truth is then transfered to paired images of three non-angiographic sequences and used to train models with a state-of-the-art segmentation architecture. We compare the results between different sequences to assess the viability and limitations of each sequence regarding practical applications. Finally, we share our ground-truth and trained models in an effort to establish a baseline dataset and method.

II. Literature Review

Moccia et al. [23] give a comprehensive overview of vessel segmentation methods for different modalities and anatomical regions. Recent contributions typically rely on the use of deep segmentation models. Hilbert et al. used the U-net architecture for the segmentation of time-of-

Manuscript received xx xx 2023; revised xx xx 2023; accepted xx xx 2023.

flight (TOF) MR angiography (MRA) [9] and anatomical labeling of 24 arterial segments [10], reporting a mean Dice similarity coefficient (DSC) of 0.93 and 0.80, respectively. Klimont et al. [20] have used the U-net architecture for the segmentation of cerebral vasculature in computed tomography (CT), based on ground-truth segmented paired CT angiography (CTA). The authors reported a mean DSC of 0.67.

To the best of our knowledge, no method has been proposed for automatic segmentation of cerebral vasculature in non-angiographic MRI.

III. Materials and Methods

For our experiments we relied on the publicly available IXI dataset [15], which comprises scans of 600 healthy patients in different modalities: TOF MRA, T1w-, T2w- and PDw-MRI. For 569 of these patients both a TOF MRA and T1w-MRI are available. The dataset has been collected using different scanning equipment at 3 different hospitals in London: Guy's Hospital (Guys), Hammersmith Hospital (HH) and Institute of Psychiatry (IOP). We generated ground-truth annotations in a fully automatic process described in the following sections.

A. Transforms, Spaces and Regions

We used the Elastix toolbox for image registration [18] to co-register the images for each patient dataset. The non-angiographic images (T1w, T2w, PDw) were aligned to the TOF MRA using a rigid parametrization derived from Timmins et al. [31]. The T1w MRI were masked using HD-BET [11] and the skull-stripped images were aligned to the symmetric MNI ICBM152 unbiased nonlinear T1w template [8] using a non-linear parametrization derived from Klein et al. [19]. We further refer to the MNI ICMBM152 template as MNI-space. For each patient, we obtain a set of transformations $\boldsymbol{T}_{T1}$, $\boldsymbol{T}_{T2}$, $\boldsymbol{T}_{PD}$ mapping the structural modalities to the TOF MRA, and $\boldsymbol{T}_{A}$, mapping from MNI-space to the T1w MRI. An overview of image spaces and transforms mapping between the spaces can be found in Figure 1.

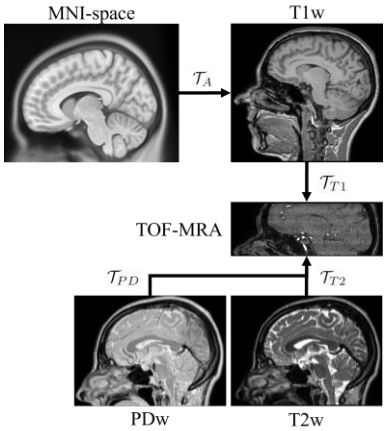

Figure 1: Image spaces and transforms at the example of patient IXI002.

Our method relies on the use of regions defined as masks in MNI-space. Each region outlines an anatomical area and can be mapped from MNI-space to any other sequence using the transforms described above. The regions were manually annotated referring to the cerebral artery probability atlas published by Mouches and Forkert [24] as outlined in Figure 2 and 3.

We define the following regions:

- R_T is the target region of the brain and supplying arteries. The region was derived from the Allen Human Reference Atlas [5], which was masked, filled and dilated to include pial arteries. The area around the carotid and basilar arteries was manually added.
- R_O is the outside region, the inverse mask of the target region R_T. The region was used to mask vessels outside the anatomical target region.
- R_{CoW} is a manually annotated region focused on the Circle-of-Willis and was used in the evaluation.
- R_C is the central region, which includes R_{CoW}, the ventricles and major supplying arteries. The region was used to filter vessels.

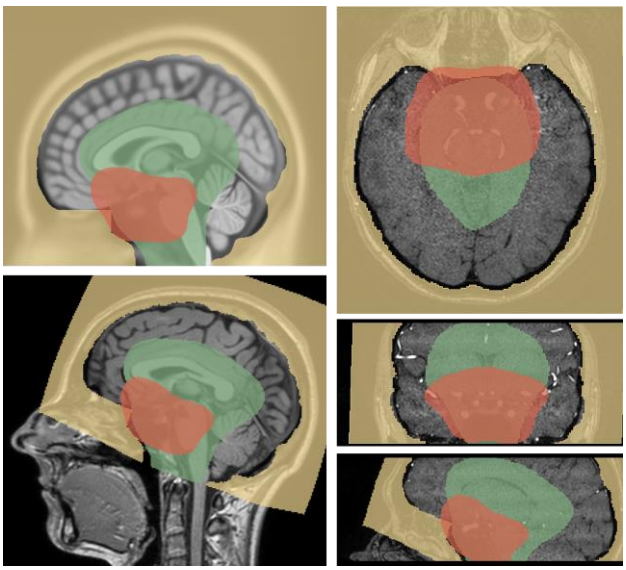

Figure 2: R_O (yellow) and R_C (green) and R_{CoW} (red) displayed on the the MNI ICMB152 template image (top left), the T1w MRI of patient IXI002 (bottom left) and planes of the respective TOF MRI (right).

Figure 3: Regions and marker positions overlayed on a volume rendering of the cerebral vessel probability atlas.

B. *Ground-Truth Generation*

We propose an automatic method to generate ground-truth for cerebral vessels. For the anatomical labeling graph- and atlas-based methods [16,25] were adapted. The ground-truth for each patient was generated using the TOF MRA and subsequently mapped to the other available modalities. Parameter-tuning was performed once for the dataset based on a template patient (IXI002). We describe our method in two steps: The segmentation of cerebral arteries and subsequent anatomical labeling. Implementation details and parameters are documented and shared with our code.

Cerebral Artery Segmentation: Each TOF MRA scan was normalized first by matching the histogram to the template patient. We applied the method of Sato et al. [27] to extract vesselness features, which were thresholded to yield a binary mask of curvilinear structures. This mask was then used to threshold bright structures within the mask. Connected-components were filtered, removing components based on their volume and median intensity, which was effective in filtering small noise particles and lower intensity structures. Regions were mapped to the scan and used for filtering. R_O was subtracted from the mask to remove vessels outside the anatomical target area. Finally, connected-components were again filtered to remove any vessels not intersecting with R_C. We further refer to the final mask as M_A.

Anatomical Labeling: Our method uses a graph representation of the vascular network to perform the anatomical labeling. Medial lines were extracted from the mask M_A using the method described by Lee et al. [21]. The medial coordinates V were then transformed into a sparse graph $G = (V,E)$, where E is a set of undirected edges e_{ij} connecting two nodes $v_i,v_j \in V$. We define d_{ij} as the Euclidean distance between both coordinates and ϕ_i as the vessel radius, which is estimated to the minimal Euclidean distance from v_i to the background of M_A. We find marker locations $M = \{m_k\} | \; m_k \in V$ in the graph map, where each marker k has been positioned within R_{CoW} in MNI-space and assigned to one of the four anatomical regions l,r,p,a (left, right, posterior, anterior) as outlined in Figure 4a. The locations m_k were transfered to patient space and assigned to the nearest medial coordinate v_i with a sufficient diameter ϕ_i above a marker dependent threshold τ_k. The markers were used to continuously search for shortest paths as the segments s outlined in Figure 4b. In an iterative process, we removed edges along the segments s_{l2}, s_{r2}, s_{la} and s_{ra} from the vessel graph until markers of distinct regions were no longer connected. Any node still connected to one of the marker nodes in the resulting G was assigned to the region of the closest one, or otherwise region n (neutral). The nodes were then used to initialize a marker-controlled watershed [4] on a boundary mask of M_A, using the medial coordinates and their assigned regions as foreground markers. The result is an annotation of M_A comprising the labels l,r,p,a and n. Figure 4c shows an exemplary result.

Screening and Selection: While our automatic method can correctly annotate different CoW types, it has a few points of failure that will lead to undesirable results. For example, poor registration will lead to displaced marker positions and ultimately cause the anatomical labeling to fail. For this reason, we assessed each scan visually for correctly labeled segments as outlined in Figure 4b. A total of 14 annotations (of 569) were excluded due to annotation errors. Figure 5 shows a selection of results including one excluded example.

Transfer to Non-Angiographic MRI: The remaining 555 annotations were mapped to the non-angiographic

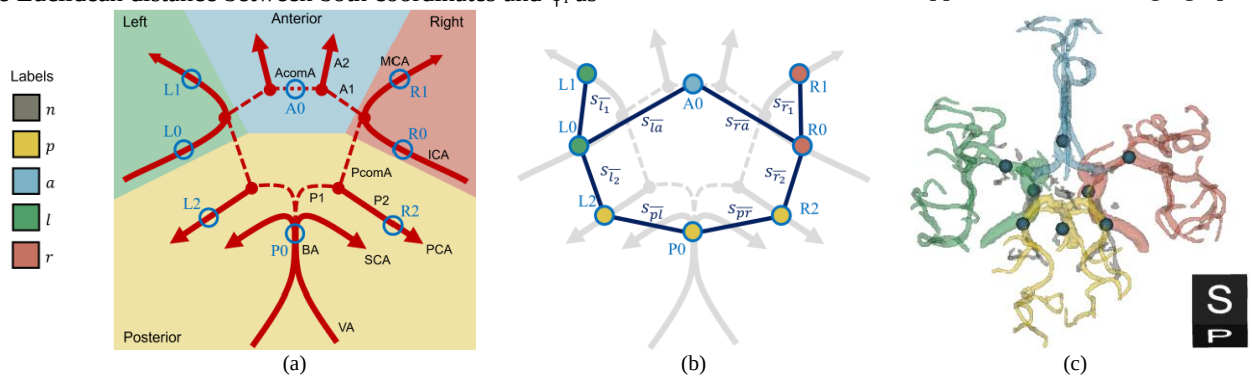

(a) (b) (c)

Figure 4: (a) An illustration of the connectivity of the primary vessels around the Circle-of-Willis. Redundant connections are marked as dashed lines, markers are shown as blue circles. (b) Paths analyzed between the markers. (c) Result segmentation for IXI002 with markers. The skeleton marker positions are shown as blue spheres.

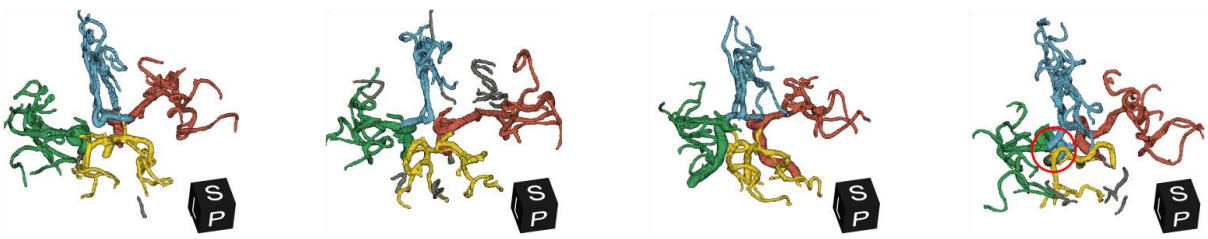

Figure 5: (From left to right) Results for IXI012, IXI459, IXI605 and IXI458 (excluded).

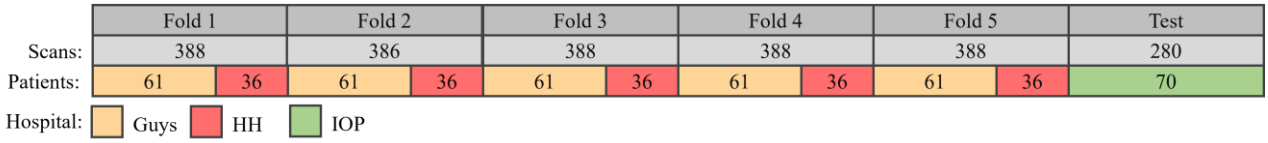

Figure 6: Outline of the 5 folds and separate test-split.

images using the respective transforms. However, to avoid any bias towards a sequence, we introduced an overlap region $R_\cap$, which is the intersection of the physical extents of all sequences of a patient. Outside $R_\cap$ the ground-truth was set to background. Each annotation label was then resampled separately using linear interpolation. The final dataset comprises 2,218 annotated scans (one patient is missing the T2w and PDw scans).

C. Training and Inference

We chose the nnU-Net [12] framework (Version 1.7.0) for training and inference. The framework has been established as a baseline for medical image segmentation and continues to achieve state of the art results in a wide range of challenges [1,13,14]. We based our configuration on the '3d_fullres' region-based trainer class for the BraTS 2020 challenge [13] and only adjusted the region definitions. The region-based setup allows the definition of region labels as a combination of one or more ground-truth labels. Labels *l,r,p,a* relate to the respective groundtruth labels, label *v* to the union of all labels (including *n*). Mirror augmentation was disabled to reduce confusions of the *l* and *r* regions. Of the 555 patients, 70 patients (280 scans) acquired by the Institute of Psychiatry (IOP) were set aside as a separate test-set. The remaining 485 patients (1.938 scans) were split into five folds as outlined in Figure 6. The nnU-Net framework automatically configured a patch size of 128x160x112 (sagittal, coronal, axial) at a spacing of 0.94 mm in-plane and 0.98 mm axial slice thickness. Training was conducted on an NVidia 1080 Ti GPU (11GB) in 1,000 epochs, each comprising 250 batches of two samples. An ensemble of all five trained models was used to predict the test-split. Figure 7 compares predictions for all modalities of two patients.

IV. Result and Discussion

We assessed the segmentation performance of our models using three metrics: the DSC, the 95th percentile of the Hausdorff distance (HD95) and the average symmetric surface distance (ASSD). For the annotation labels we evaluated the mean DSC. The scores were calculated within the intersection region $R_\cap$ of each patient and a second time for the region R_{CoW} to outline the performance around the critical CoW structures. The evaluation results for each metric and label grouped by sequence are outlined in Figure 8 and averaged over modalities and labels in Table 2. The segmentation performance is promising with a DSC of 0.75 and 0.82 for the full and CoW region, respectively. The performance drops considerably for the test-split, although not as significant for the CoW region, which suggests that the MRI acquisition protocol has a strong effect. Ordered by DSC score, the sequences rank TOF MRA, PDw, T2w and T1w with scores 0.84, 0.75, 0.72 and 0.71 in the full region or 0.89, 0.82, 0.80 and 0.78 in the CoW region. We compare our results to several related methods in Table 2, of which Klimont et al. [20] is the only method for non-angiographic (CT) images. The comparability between the methods is limited as the complexity of the segmentation task heavily depends on the modality, the anatomical region, the labeled anatomy and sparsity of the ground-truth. Furthermore, distance-based metrics would provide a better indication of segmentation quality than DSC scores [2] but are only given by Hilbert et al. [10], which we outperformed in the HD95 score. For the TOF MRA, our DSC segmentation score is comparably low with 0.84 (0.89 for the CoW region), which can in part be attributed to the relatively low physical resolution of the model. We generally observed a significant amount of over-segmentation in

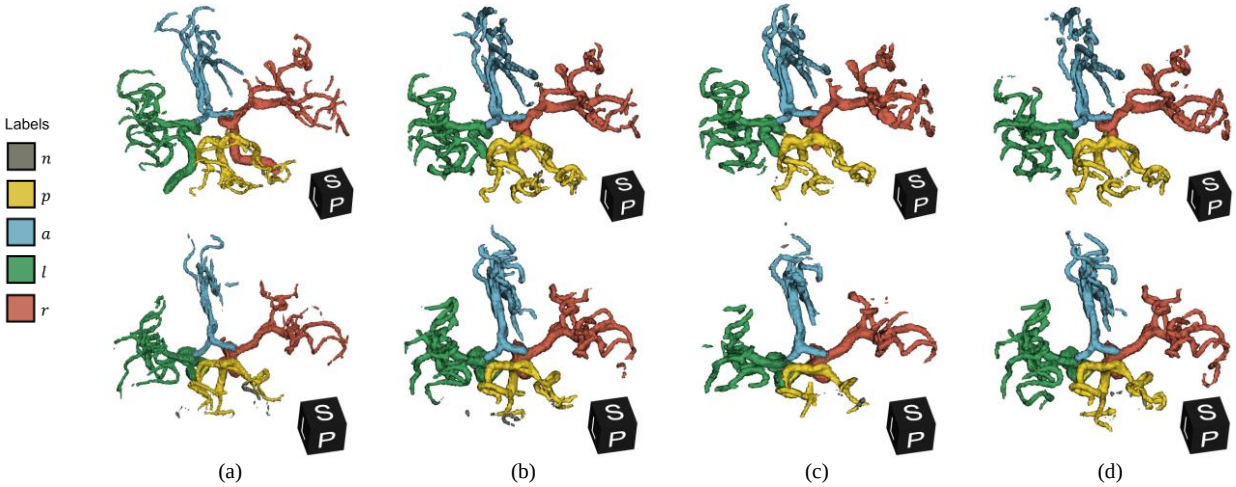

(a) (b) (c) (d)

Figure 7: Predictions for (a) TOF MRA, (b) PDw, (c) T1w and (d) T2w of IXI002 of the validation-split (top) and IXI347 of the test-split (bottom).

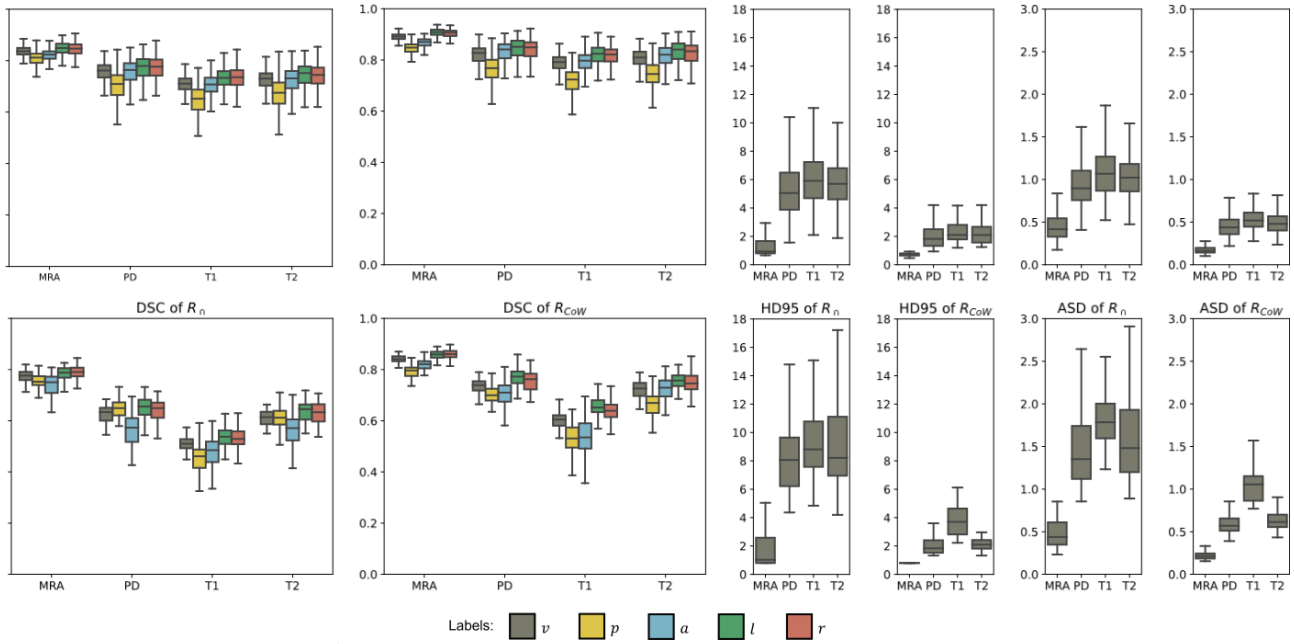

Figure 8: Evaluation metrics for the cross validation (top) and test-split (bottom) Table 1: The evaluation metrics over all sequences.

the region outside the CoW where ground-truth is sparse. Further details are outlined in our Supplementary Materials.

TABLE 9: THE EVALUATION METRICS OVER ALL SEQUENCES.

Split	Region	ASSD	HD95	DSC	
				v	*l,r,p,a*
Validation	Full	0.90±0.39	4.81±2.85	0.75±0.06	0.75±0.08
	CoW	0.44±0.25	1.99±1.62	0.82±0.07	0.82±0.06
Test	Full	1.38±0.70	7.26±4.19	0.63±0.10	0.62±0.11
	CoW	0.65±0.38	2.53±2.02	0.75±0.24	0.72±0.11

TABLE 10: COMPARISON TO RELATED METHODS OF CEREBRAL ARTERY SEGMENTATION AND ANNOTATION. ALL VALUES REFER TO THE REPORTED CROSS-VALIDATION EXPERIMENTS.

Method	Model	Scans	Modality	Label	DSC	HD95
Ours	U-Net	1,938	Multiple	4	0.75	4.80
Hilbert et al. [9]	U-Net	264	MRA	1	0.93	29.15
Hilbert et al. [10]	U-Net	242	MRA	26	0.80	-
Sobisch et al. [29]	PointNet	152	MRA	6	0.91	-
Yao et al. [33]	GCN	72	CTA	13	0.90	-
Klimont et al. [20]	U-Net	120	CT	1	0.67	-

V. CONCLUSION

We presented a fully automatic method to segment and annotate cerebral arteries in four different MRI sequences. While the non-angiographic sequences were outperformed by the TOF MRA baseline, the results are definitely viable for all sequences with cross validation DSC scores consistently over the often-cited threshold of 0.7 [3]. However, the evaluation on the separate test-split suggests further training on a larger variety of sequences to improve generalization. In that regard, our automatic ground-truth generation method can be applied to annotate additional datasets and potentially be improved to capture smaller vessels more consistently or annotate arterial segments. Our work suggests the utility of non-angiographic sequences for automated vessel segmentation and annotation. We recommend its use for the assessment of larger cerebral arteries, e.g., for orientation or to improve the alignment of angiography images. In our future work, we will extend our training with pathological images to explore the viability of non-angiographic sequences for the assessment of cerebrovascular disease. We share our trained models with code to reproducing our experiments publicly at https://github.com/risc-mi/cerebral-artery-annotation.

APPENDIX A: GROUND-TRUTH GENERATION

Figure 11 shows a step-for-step outline of our ground-truth generation method at the example of IXI002: (a) Volume rendering of the TOF MRA, (b) the vesselness response, (c) the inital mask, (d) after filtering connected-components, (e) after region-based filtering, (f) with anatomical labels.

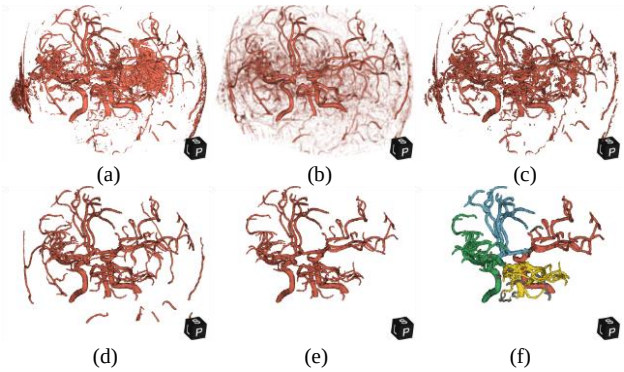

Figure 11: Ground-Truth Generation

APPENDIX B: ACCURACY OF MEDIAL COORDINATES

Figure 12 shows the accuracy of predicting the ground-truth medial coordinates *V*. The accuracy is given as the ratio of $v_i \in V$ segmented in the prediction (region-label *v*). Results are shown for each modality, region ($R_\cap$ or R_{CoW}) and dataset (cross-validation or test-split).

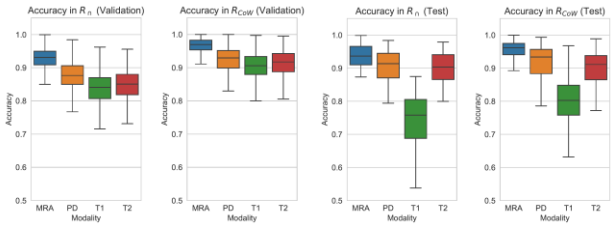

Figure 12: Accuracy as the ratio of predicted medical coordinates v_i.

Figure 13 shows results for ground-truth medial coordinates V in relation to their estimated radius. True-Positives (TN) and False-Negatives (FN) indicate whether a coordinate v_i of radius ϕ_i was segmented in the prediction (region-label v).

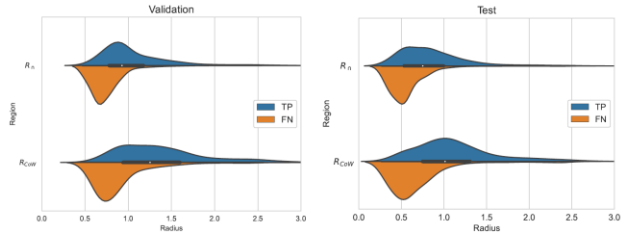

Figure 13: TN and FN for coordinates v_i in relation to their respective radius ϕ_i.

Conflict of Interest

The authors declare no conflict of interest.

Author Contributions

Bertram Sabrowsky-Hirsch conducted the research and wrote the paper in collaboration with Phillip Moser, Stefan Thumfart and Josef Scharinger. All authors had approved the final version.

Funding

This work was funded by the FFG (Austrian Research Promotion Agency) under the grant 872604 (MEDUSA) and research subsidies granted by the government of Upper Austria. RISC Software GmbH is a member of UAR (Upper Austrian Research) Innovation Network.

References

1. M., Antonelli, *et al.*: *The Medical Segmentation Decathlon*. Nature Communications 13(1), 4128 (2022).
2. O.U., Aydin, *et al.*: *An evaluation of performance measures for arterial brain vessel segmentation*. BMC Medical Imaging 21(1), 113 (2021).
3. J.J., Bartko: *Measurement and Reliability: Statistical Thinking Considerations*. Schizophrenia Bulletin 17(3), 483–489 (1991).
4. R., Beare, *et al.*: *Brain extraction using the watershed transform from markers*. Frontiers in neuroinformatics 7, 32 (2013)
5. S., Ding, *et al.*: *Allen human reference atlas–3d*, 2020. RRID: SCR_017764 (2020), Version 1.0.0
6. T., Dobrocky, *et al.*: *Benefit of advanced 3d dsa and mri/ct fusion in neurovascular pathology*. Clinical neuroradiology pp. 1–8 (2023)
7. T.L., Fauber, M.C., Dempsey: X-ray field size and patient dosimetry. Radiologic Technology 85(2), 155–161 (2013)
8. V., Fonov, *et al.*: *Unbiased average age-appropriate atlases for pediatric studies*. NeuroImage 54(1), 313–327 (2011).
9. A., Hilbert, *et al.*: Brave-net: *Fully automated arterial brain vessel segmentation in patients with cerebrovascular disease*. Frontiers in Artificial Intelligence 3 (2020).
10. A., Hilbert, *et al.*: *Anatomical labeling of intracranial arteries with deep learning in patients with cerebrovascular disease.* Frontiers in Neurology 13 (2022).
11. F., Isensee, *et al.*: Automated brain extraction of multisequence mri using artificial neural networks. Human Brain Mapping 40(17), 4952–4964 (2019).
12. F., Isensee, *et al.*: nnu-net: *a self configuring method for deep learning-based biomedical image segmentation*. Nature methods 18(2), 203–211 (2021).
13. F., Isensee, *et al.*: *nnU-Net for Brain Tumor Segmentation*. Brainlesion: Glioma, Multiple Sclerosis, Stroke and Traumatic Brain Injuries. pp. 118–132. Lecture Notes in Computer Science, Springer, Cham (2021).
14. F., Isensee, *et al.*: *Extending nnu-net is all you need*. Bildverarbeitung für die Medizin 2023. BVM 2023. Informatik aktuell. Springer, Wiesbaden. (2022).
15. *The information extraction from images (ixi) dataset.* https:// brain-development.org/ixi-dataset/, Accessed 09 Jul 2022
16. J., Kassam, *et al.*: *Detecting large vessel occlusions using graph deep learning*. Geometric Deep Learning in Medical Image Analysis. pp. 149–159. PMLR (2022)
17. M., Katan, A., Luft: Global Burden of Stroke. Seminars in Neurology 38(2), 208–211 (2018). https://doi.org/10.1055/s-0038-1649503
18. S., Klein, *et al.*: *Elastix: A toolbox for intensity-based medical image registration*. IEEE Transactions on Medical Imaging 29(1), 196–205 (2010).
19. S., Klein, *et al.*: Automatic segmentation of the prostate in 3d mr images by atlas matching using localized mutual information. Medical physics 35(4), 1407–1417 (2008).
20. M., Klimont, *et al.*: Deep learning for cerebral angiography segmentation from non-contrast computed tomography. PLoS ONE 15(7) (2020).
21. T., Lee, R., Kashyap, C., Chu: *Building skeleton models via 3-d medial surface axis thinning algorithms*. CVGIP: Graphical Models and Image Processing 56(6), 462–478 (1994).
22. B.J., MacIntosh, S.J., Graham,: *Magnetic Resonance Imaging to Visualize Stroke and Characterize Stroke Recovery: A Review*. Frontiers in Neurology 4 (2013).
23. S., Moccia, *et al.*: *Blood vessel segmentation algorithms — Review of methods, datasets and evaluation metrics*. Computer Methods and Programs in Biomedicine 158, 71–91 (2018).
24. P., Mouches, N.D., Forkert: *A statistical atlas of cerebral arteries generated using multi-center mra datasets from healthy subjects.* Scientific data 6(1), 29 (2019).
25. N., Passat, *et al.*: *Region growing segmentation of brain vessels: an atlas-based automatic approach*. JMRI21(6) (2005).
26. H., Sarikaya, *et al.*: *Outcomes of intravenous thrombolysis in posterior versus anterior circulation stroke*. Stroke 42(9), 2498–2502 (2011).

27. Y., Sato, *et al.*: *Three-dimensional multi-scale line filter for segmentation and visualization of curvilinear structures in medical images*. Medical Image Analysis 2(2), 143–168 (1998).
28. E.E., Smith, *et al.*: *Prevention of Stroke in Patients with Silent Cerebrovascular Disease*: A Scientific Statement for Healthcare Professionals from the American Heart Association/American Stroke Association. Stroke 48(2), e44–e71 (2017).
29. J., Sobisch, *et al.*: *Automated intracranial vessel labeling with learning boosted by vessel connectivity, radii and spatial context.* Geometric Deep Learning in Medical Image Analysis. pp. 34–44. PMLR (2022) 30. Tedyanto, E.H., et al.: Magnetic Resonance Imaging in Acute Ischemic Stroke. Cureus 14(7) (2022).

[31] K.M., Timmins, *et al.*: *Comparing methods of detecting and segmenting unruptured intracranial aneurysms on tof-mras*: The adam challenge. NeuroImage 238, 118–216 (2021).

[32] J.M., Wardlaw, *et al.*: *Neuroimaging standards for research into small vessel disease and its contribution to ageing and neurodegeneration.* The Lancet Neurology 12(8), 822–838 (2013).

[33] L., Yao, *et al.*: *Graph Convolutional Network Based Point Cloud for Head and Neck Vessel Labeling*. Machine Learning in Medical Imaging. pp. 474–483. Lecture Notes in Computer Science, Springer International Publishing, Cham (2020).

Bertram Sabrowsky-Hirsch received the MSc degree from the University of Applied Sciences Upper Austria, in 2016. He is currently pursuing the PhD Degree from the Institute of Computational Perception, Johannes Kepler University Linz while being employed at the Unit for Medical Informatics at RISC Software GmbH. His research is centered around Deep Learning for Medical Image Analysis.